Journal of Solid State Chemistry **155,** 381–388 (2000)
doi:10.1006/jssc.2000.8928, available online at http://www.idealibrary.com on IDEAL®

Structural Phase Transitions in $Sr_2Fe_2O_5$ under High Pressure

P. Adler, U. Schwarz,[1] and K. Syassen

Max-Planck-Institut für Festkörperforschung, Heisenbergstr. 1, D-70569 Stuttgart, Germany

E-mail: adler@sim.mpi-stuttgart.mpg.de

A. P. Milner and M. P. Pasternak

School of Physics and Astronomy, Tel Aviv University, 69978 Tel Aviv, Israel

E-mail: hh136@post.tau.ac.il

and

M. Hanfland

European Synchrotron Radiation Facility, BP 220, F-38043 Grenoble, France

Received May 30, 2000; in revised form August 1, 2000; accepted August 9, 2000; published online November 29, 2000

The pressure dependence of the crystal structure of $Sr_2Fe_2O_5$ has been studied at room temperature by angle-dispersive synchrotron X-ray powder diffraction and ^{57}Fe Mössbauer spectroscopy using diamond anvil cell techniques. Between 11 and 14 GPa the low-pressure brownmillerite-type structure with an equal number of octahedrally and tetrahedrally coordinated Fe^{3+} sites is transformed into a tetragonal perovskite-like structure. The Mössbauer spectra of the high-pressure phase reveal two subspectra with an intensity ratio of about 3:1. The Mössbauer parameters are consistent with two five-coordinated Fe^{3+} sites differing in the degree of structural distortion of the FeO_5 polyhedra. Laser annealing of the high-pressure phase at 15 GPa induces a transformation from the tetragonal perovskite into an orthorhombic phase that is isostructural with $Sr_2Mn_2O_5$. This structure consists of a network of corner-sharing FeO_5 square pyramids. The coordination number of the Sr^{2+} ions has increased from 8 in the brownmillerite structure to 10 in the $Sr_2Mn_2O_5$-type phase. © 2000 Academic Press

Key Words: **iron oxides; powder X-ray diffraction; Mössbauer spectroscopy; high pressure; phase transitions.**

1. INTRODUCTION

Several transition metal oxides with composition $A_2M_2O_5$ crystallize in oxygen-deficient perovskite structures that differ in the ordering patterns of anion vacancies. Well-known examples are oxoferrates $A_2Fe_2O_5$ with A = Ca, Sr (1–4). These compounds crystallize in brownmillerite(B)-type structures that are composed of perovskite-like layers with corner-sharing MO_6 octahedra ($M^{3+}(O)$ ions) alternating with slabs containing rows of corner-sharing MO_4 tetrahedra ($M^{3+}(T)$ ions). The crystal structures of $Sr_2Fe_2O_5$ (4) (space group *Ibm*2) and $Ca_2Fe_2O_5$ (1) (space group *Pcmn*) are similar but differ in the orientation of successive FeO_4 tetrahedra along the *b* axis. An illustration of the crystal structure of $Sr_2Fe_2O_5$ is given in Fig. 1 (top). Also $Ba_2Fe_2O_5$ is known and was initially believed to be isostructural to $Ca_2Fe_2O_5$ (5). However, subsequent structural and Mössbauer studies of $Ba_2Fe_2O_5$ point to a complex perovskite-related defect structure with a coexistence of O, T, and five-coordinated Fe^{3+} sites in the ratio 3 : 3 : 1 (6, 7). Another kind of vacancy ordering is encountered in oxomanganates $A_2Mn_2O_5$ (A = Ca, Sr) where the Mn^{3+} ions exclusively reside in five-coordinated square-pyramidal sites (8, 9) (see Fig. 1, bottom). We also mention $La_2Ni_2O_5$ where slabs of $Ni^{2+}(O)$ sites are connected by Ni^{2+} ions in square planar coordination environments of oxygen ions (10).

The various ways of distributing oxygen vacancies in $A_2M_2O_5$ defect perovskite materials suggests the possibility of temperature- and pressure-induced phase transitions. Indeed, temperature-dependent X-ray diffraction (XRD) and differential thermoanalysis (DTA) studies of $Sr_2Fe_2O_5$ revealed structural phase transitions at elevated temperatures (11–13). There is, however, disagreement about the detailed

[1] Current address: Max-Planck-Institut für Chemische Physik fester Stoffe, Pirnaer Landstraße 176, D-01257 Dresden, Germany.

0022-4596/00 $35.00

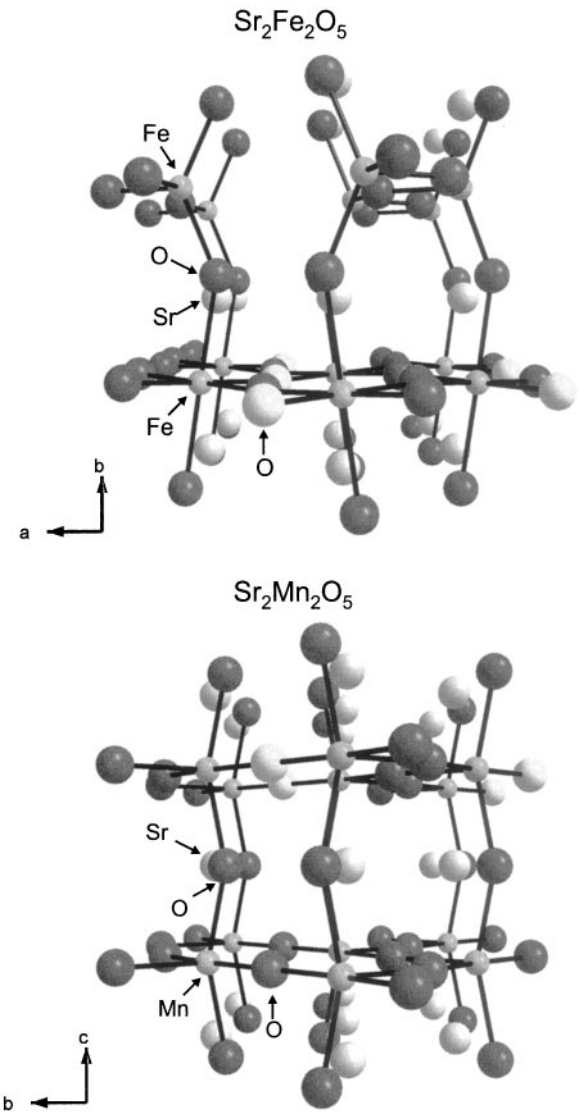

FIG. 1. Details from the crystal structures of $Sr_2Fe_2O_5$ (top) and $Sr_2Mn_2O_5$ (bottom). In $Sr_2Fe_2O_5$ perovskite-like layers of FeO_6 octahedra alternate with sheets containing rows of corner-sharing FeO_4 tetrahedra. $Sr_2Mn_2O_5$ reveals a network of corner-sharing MnO_5 square pyramids. Highlighted oxygen atoms serve for comparison between the two crystal structures (see Section 3.4).

transition temperatures and phases. Shin *et al.* (11) reported a change from a brownmillerite to a cubic perovskite (P) phase for $Sr_2Fe_2O_5$ near 973 K. Two crystallographic phase transitions near 623 and 1123 K were established by Grenier *et al.* (12). The first transition leads to a mixture of the B-type and a tetragonal perovskite (Q) phase, the second transition revealed a hysteresis, and a cubic perovskite phase was observed above 1123 K. On the other hand, in the study by Takeda *et al.* (13) only one phase transition from the B-type to a cubic perovskite phase was found. For explaining the discrepancies between the various studies, deviations from ideal stoichiometry were proposed as $Sr_2Fe_2O_5$ readily takes up oxygen. Also the microscopic consequences of the structural changes are not yet clear. Whereas Shin *et al.* (11) suggest an order–disorder transition leading to a random distribution of oxygen vacancies, Grenier *et al.* (12) favor a structural model involving the formation of microdomains that still have the B-type structure. At the domain boundaries the disappearance of *T* and *O* sites and the formation of five-coordinated Fe^{3+} sites were considered as likely. Temperature-dependent ^{57}Fe Mössbauer spectra of $Sr_2Fe_2O_5$ up to 1223 K (14, 15) reveal no major changes that can be associated with structural phase transitions. A second-order structural phase transition with a change in space group from *Pcmn* to *Icmm*, which mainly affects the FeO_4 tetrahedra and the coordination polyhedra around the Ca^{2+} ions, was derived recently from a temperature-dependent neutron diffraction study of $Ca_2Fe_2O_5$ (16).

In view of the coexistence of six- and four-coordinated Fe^{3+} sites in the crystal structures of the B-type phases it is interesting to investigate how these compounds behave under high pressure. According to a common rule in crystal chemistry high pressure favors the formation of structures with increased coordination numbers for one or more of the atoms.

We have studied the pressure dependence of the crystal structure of $Sr_2Fe_2O_5$ at room temperature by angle-dispersive X-ray (synchrotron) powder diffraction and by ^{57}Fe Mössbauer spectroscopy. In addition, XRD diagrams of $Sr_2Fe_2O_5$ were measured at several pressures after heating the sample by laser annealing. Our experimental data evidence structural phase transitions at high pressures involving a change in the coordination environments of the Fe^{3+} ions.

2. EXPERIMENTAL

$Sr_2Fe_2O_5$ was prepared from a 2:1 mixture of SrO (stored under argon) and Fe_2O_3 that was thoroughly ground in an agate mortar under an inert argon atmosphere of a glove box. The mixture was transferred to a quartz tube and heated to 1373 K at an argon pressure of about 100 mbar. After 12 h the sample was cooled, reground, pressed into pellets, and heated under the same conditions for 5 days. For high-pressure Mössbauer experiments a powder sample of $Sr_2Fe_2O_5$ was prepared that was enriched to a content of 25% ^{57}Fe. In this case a mixture of SrO and appropriate amounts of Fe_2O_3 and $^{57}Fe_2O_3$ were quickly mixed in air and the reaction temperature was 1273 K. The samples were shown to be single phase by powder XRD using monochromatic Cu$K\alpha_1$ radiation. The lattice parameters of the sample with natural abundance of Fe isotopes that was used for the XRD studies were $a = 567.39(3)$ pm, $b = 1557.7(1)$

pm, and $c = 552.85(3)$ pm. Room-temperature Mössbauer spectra of both samples reveal only Fe^{3+} and no Fe^{4+} signals.

The pressure dependence of the crystal structure of $Sr_2Fe_2O_5$ was investigated by angle-dispersive powder X-ray diffraction at the ID9 undulator beamline of the European Synchrotron Radiation Facility (ESRF), Grenoble. Finely ground samples of $Sr_2Fe_2O_5$ were loaded into the gasket hole of a diamond anvil cell (DAC) using nitrogen or argon as the pressure-transmitting medium. Two-dimensional diffraction patterns were measured with X-ray wavelengths of 45.80 and 45.86 pm using image plate detection. In order to improve powder averaging the DAC was rotated by $\pm 3°$. Typical data collection times were 2 to 4 min. The scanned two-dimensional images were corrected for tilt and scanner distortions and converted to intensity vs 2Θ data using the Fit2D software (17). In one set of experiments XRD patterns without thermal treatment were collected at room temperature (pressure medium, nitrogen). In order to further investigate the nature of a structural phase transition seen in the XRD and Mössbauer data a second set of experiments was performed on another sample (pressure medium, argon). In this case the compound was first pressurized to about 15 GPa for converting $Sr_2Fe_2O_5$ into the high-pressure phase. Subsequently the sample was annealed by irradiation with a Nd-YAG laser for 1 min. The sample temperature during laser irradiation was estimated as 800°C. Two further annealing experiments at about 20 and 23 GPa were carried out. Full-profile refinements of the powder patterns were performed using the FullProf (18) and GSAS (19) programs. As the quality of the present data is not sufficient for a complete refinement of all atomic positions (in particular of the oxygen positions) we focus here only on a discussion of the lattice parameters. Therefore no details from the structural evaluations are tabulated.

Pressure-dependent ^{57}Fe Mössbauer experiments were performed with the sample deposited in a miniature DAC with 0.5-mm culets and a cavity 0.25 mm in diameter and 0.03 mm in height drilled into a TaW gasket. Argon was used as the pressure medium. Spectra up to 25 GPa were obtained using a 10-mCi ^{57}Co(Rh) point source. All spectra were analyzed using appropriate least-squares-fitting procedures for deriving the hyperfine interaction parameters. Isomer shift data are referred to α-iron.

3. RESULTS AND DISCUSSION

3.1. XRD Studies without Laser Annealing

For $P \leq 11$ GPa the XRD diagrams (Fig. 2) are characteristic of the B-type phase of $Sr_2Fe_2O_5$. The pressure dependence of the lattice parameters in this region was obtained from Rietveld calculations within the space group *Ibm*2 which was derived from a single crystal structure determination of $Sr_2Fe_2O_5$ (4). The peak shapes were described by a modified Lorentzian (mod 2) profile function (20). Refinements included the scale factor, background, and lineshape parameters; the orthorhombic lattice parameters *a*, *b*, and *c*; and the positional parameters of the Sr and Fe ions. The positional parameters of the oxygen atoms were fixed to the values from the single crystal study (4). Powder diagrams of $Sr_2Fe_2O_5$ up to 11 GPa are well reproduced by this structural model.

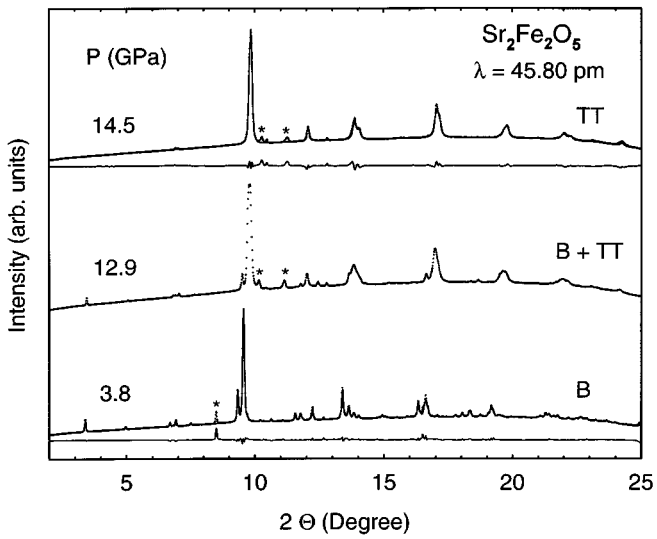

FIG. 2. Powder XRD patterns of $Sr_2Fe_2O_5$ at room temperature for different pressures. Solid lines show results from Rietveld calculations (3.8 GPa: $a_B = 562.7$ pm, $b_B = 1542.5$ pm, $c_B = 548.1$ pm, $R_I = 0.09$, $R_{wp} = 0.11$; 14.5 GPa: $a_{TT} = 379.4$ pm, $c_{TT} = 374.3$ pm, $R_I = 0.13$, $R_{wp} = 0.14$; esd's ≤ 0.1 pm). Bottoms of the diagrams show difference curves between experimental data and calculated profiles. Reflections marked by an asterisk are due to diffraction from the nitrogen matrix. Abbreviations used: B, brownmillerite-type, TT, tetragonal perovskite-type phase.

At pressures *P* between about 11 and 14 GPa a structural phase transition is observed. The XRD diagram at 12.9 GPa corresponds to a superposition of the low- and high-pressure patterns. At $P \geq 14$ GPa the XRD patterns are more simple. Several reflections have disappeared, which is particularly evident in the 2Θ region below 10°; others have merged together. The XRD diagrams are indicative of a perovskite structure. Peak splitting evidences departure from cubic symmetry and suggests a tetragonal unit cell. For obtaining the pressure dependence of the lattice parameters the experimental patterns for $P \geq 14$ GPa were modeled with the assumption of a tetragonally distorted primitive perovskite-type cell. It cannot be excluded, however, that the true symmetry is lower. Preferred orientation along [111] was taken into account. After pressure release the diagram of the B phase was recovered ensuring the reversibility of the phase transition.

At this point it is noted that all diagrams reveal additional weak reflections that show a different pressure dependence

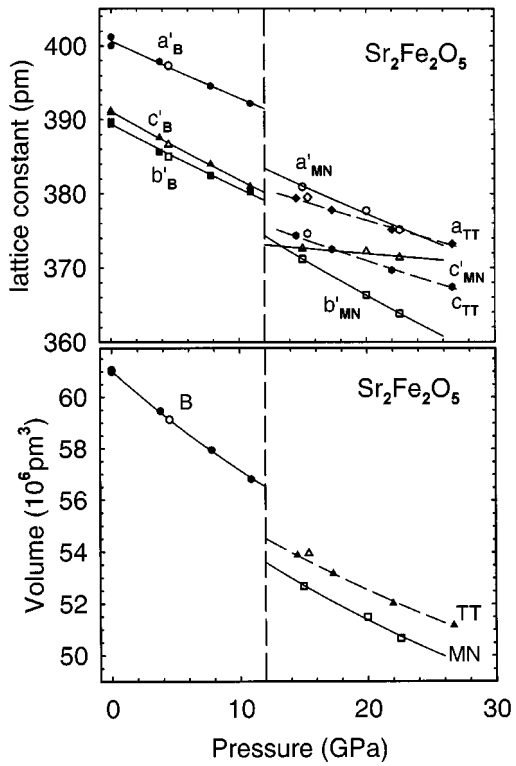

FIG. 3. Lattice parameters (top) and volume V (bottom) of a primitive perovskite-type unit cell as a function of pressure. Closed symbols correspond to the first set of experiments; open symbols correspond to the second set of experiments (see Sections 3.1 and 3.3, respectively). Solid lines are the best fits of a Murnaghan-type equation to the experimental data. Abbreviations used: *B*, brownmillerite-type; TT, tetragonal perovskite-type; MN, $Sr_2Mn_2O_5$-type phase.

and are attributed to diffraction from the nitrogen matrix. Considering the possibility of superstructure reflections in the high-pressure phase it is emphasized that no additional reflections in the range of small 2Θ that correspond to large d values were observed.

It is concluded that between 11 and 14 GPa the orthorhombic brownmillerite (B) structure is transformed into a tetragonal perovskite-like (TT) structure. The lattice constants a_B, b_B, and c_B of the B phase are related to the lattice parameter a_P of a cubic perovskite structure by the relations $a_B \approx \sqrt{2}a_P$, $b_B \approx 4a_P$, and $c_B \approx \sqrt{2}a_P$. In Fig. 3 the reduced lattice parameters $a'_B = a_B/\sqrt{2}$, $b'_B = b_B/4$, and $c'_B = c_B/\sqrt{2}$ of the B phase as well as the parameters a_{TT} and c_{TT} of the TT phase are depicted as a function of pressure. In the B phase the differences between b'_B and c'_B are small, whereas the a'_B values are considerably larger. All three lattice parameters decrease with pressure to a similar extent. In the TT phase a_{TT} roughly adopts values as expected from an extrapolation of the b'_B and c'_B parameters to higher pressures. The c_{TT} parameters are smaller than the a_{TT} parameters. The pressure trends in the reduced lattice parameters result in a discontinuity for the pressure dependence of the volume V (Fig. 3). The $V(P)$ data of the low-pressure (LP) B and high-pressure (HP) TT phase were described by a Birch–Murnaghan equation of state,

$$V/V_0 = [1 + (B'/B_0)(P - P_0)]^{-1/B'}, \qquad [1]$$

where V_0, B_0, and B' are volume, bulk modulus, and its pressure derivative at $P_0 = 0$ GPa and $P_0 = 12$ GPa for the B and TT phases, respectively. Corresponding equations were used for fitting the pressure dependence of the lattice constants. The results from the $V(P)$ fits obtained with the standard value $B' = 4$ are given in Table 1. The discontinuous decrease in V by $-3.6 \pm 0.5\%$ at 12 GPa indicates that the structural phase transition is of first order.

3.2. *Mössbauer Spectroscopy*

Mössbauer spectra of $Sr_2Fe_2O_5$ under pressure at room temperature were measured to obtain information about the coordination environments of the Fe^{3+} ions in the TT phase (see Fig. 4). Up to about 6 GPa the spectra consist of two subspectra α and β with equal abundance, in agreement with earlier results at ambient pressure (2). The spectra reflect the coexistence of $Fe^{3+}(T)$ and $Fe^{3+}(O)$ sites in the B-type crystal structure of $Sr_2Fe_2O_5$. The six-line pattern for each site is due to hyperfine splitting as $Sr_2Fe_2O_5$ is antiferromagnetic below $T_N = 715$ K (3). Subspectrum α with smaller isomer shift (IS) and hyperfine field (B_{hf}) values corresponds to $Fe^{3+}(T)$ sites; subspectrum β with larger IS and B_{hf} values corresponds to $Fe^{3+}(O)$ sites. The presence of a quadrupole interaction ε is in agreement with the significant distortion of octahedra and tetrahedra that is apparent from the iron–oxygen distances (4). From a single-crystal Mössbauer study of $Ca_2Fe_2O_5$ (21) it was shown that the electric field gradient (efg) tensors are approximately axially symmetric for both Fe sites. The principal components $V_{zz} = eq$ are parallel to the b axis. We assume this to be the case also in $Sr_2Fe_2O_5$. For an axially symmetrical efg, ε is defined by

$$\varepsilon = e^2qQ(3\cos^2\Theta - 1)/8, \qquad [2]$$

TABLE 1

Parameters Obtained from a Fit of a Birch–Murnaghan-Type Equation (See Eq. [1]) with $B' = 4$ to the Volume $V(P)$ of a Primitive Perovskite-Type Unit Cell for the Different Phases of $Sr_2Fe_2O_5$

Phase	P_0 (GPa)	V_0 (10^6 pm^3)	B_0 (GPa)
B	0	61.0(1)	133(3)
TT	12	54.5(1)	200(7)
MN	12	53.6(2)	173(20)

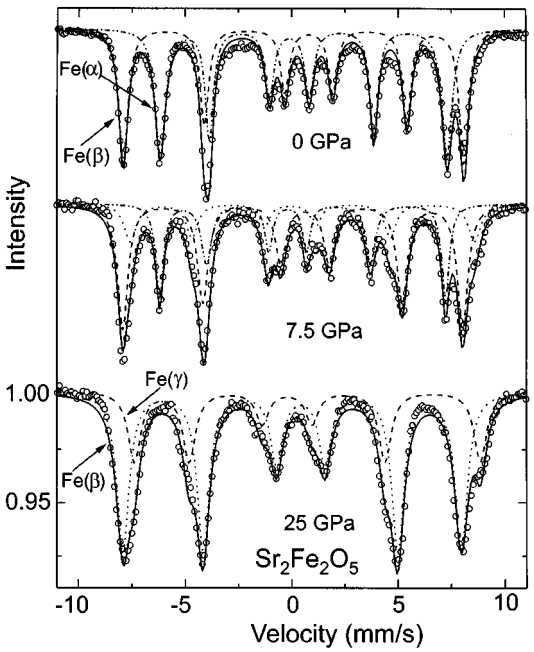

FIG. 4. ^{57}Fe Mössbauer spectra of $Sr_2Fe_2O_5$ at room temperature for various pressures. Solid lines correspond to Lorentzian fits to the data; subspectra are indicated by dashed and dotted lines.

where Q is the nuclear quadrupole moment and Θ is the angle formed between B_{hf} and V_{zz}. The experimental results show that ε is negative for the O sites and positive for the T sites. As the spins are oriented along the c axis (namely $\Theta = 90°$) this leads to the conclusion that V_{zz} is positive for the Fe(O) and negative for the Fe(T) sites, respectively. In this case the quadrupole splitting QS is given by $4|\varepsilon|$.

At $P > 6$ GPa an additional subspectrum γ appears, concurrent with a decrease in the intensity (abundance) of the α component. Between 6 and 13 GPa the spectra reveal three components: α, β, and γ. Above 13 GPa there are no major changes in the spectral shapes and the spectra are well described by two components β and γ with an intensity ratio of approximately 3:1. The $Fe^{3+}(T)$ component α has completely vanished. The changes in the Mössbauer spectra appear in a similar pressure range where structural changes were observed in the XRD diagrams and thus are attributed to the structural phase transition from the B-type to the TT phase. Actually in the Mössbauer spectra the phase transition is seen at about 3 GPa pressures lower than in the XRD experiments. This may be partly due to local strains arising from different ways of packing of the powder particles in the two experiments. Furthermore, Mössbauer spectroscopy is a local probe whereas XRD experiments lead to spatial averaging. We believe this to be the reason that changes in the Mössbauer spectra are seen over a broader range of pressures.

The pressure dependence of the various Mössbauer parameters is depicted in Fig. 5. In the absence of a phase transition it is expected that IS decreases with increasing P due to an increasing s-electron density $\rho_s(0)$ at the nucleus. Indeed, this behavior is observed for all components in the spectra (Fig. 5a). However, the IS(β) data show a pronounced change in the pressure range of the phase transition. Extrapolation of the IS values of the pure LP and HP phases reveals that for a given pressure the IS(β) values in the HP phase are intermediate between the smaller IS(α)

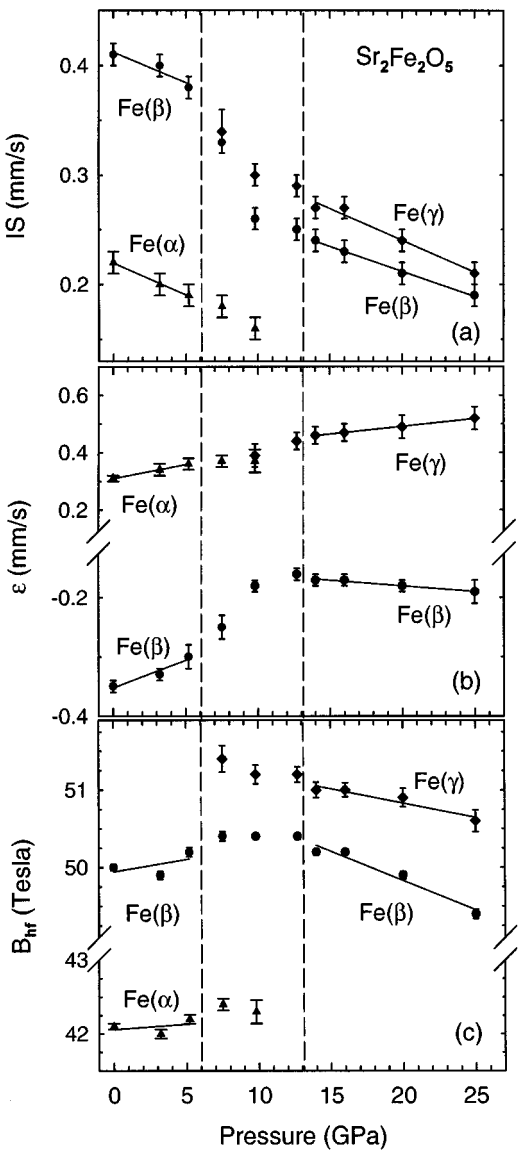

FIG. 5. Pressure dependence of (a) isomer shifts IS, (b) quadrupole interaction parameters ε, and (c) hyperfine fields B_{hf} for the different Fe sites of $Sr_2Fe_2O_5$. The solid lines emphasize the trends in the low-pressure B phase and high-pressure TT phase. The pressure range of the phase transition seen in Mössbauer spectroscopy is indicated by the dashed lines.

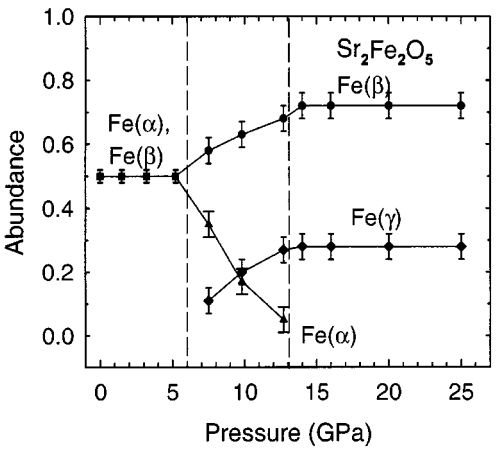

FIG. 6. Pressure dependence of the abundance of the different Fe sites calculated from the area fractions of the Mössbauer spectra. The solid lines are guides to the eye. The pressure range of the phase transition is indicated by the dashed lines.

and the larger IS(β) values in the LP phase. As subspectra α and β in the LP phase correspond to the four-coordinated $Fe^{3+}(T)$ and and the six-coordinated $Fe^{3+}(O)$ sites, repectively, it is concluded that subspectrum β in the HP phase arises from five-coordinated $Fe^{3+}(5)$ ions. In the pressure range of the phase transition the IS(β) values are in between the larger LP and smaller HP values. No additional components are resolved in the spectra recorded at pressures within the phase-transition range. The IS values of subspectrum γ are similar to the HP values of subspectrum β which suggests that the second Fe species corresponds to $Fe^{3+}(5)$ ions too.

A pronounced change is also apparent in the pressure dependence of the quadrupole interaction parameter $\varepsilon(\beta)$ (Fig. 5b) with $|\varepsilon|(\beta)$ in the HP phase being only half as large as in the LP phase. The sign of $\varepsilon(\beta)$ is negative in both phases. If the efg is still approximately axially symmetric and if the spin orientation remains unchanged during the phase transition, then a decrease in $|\varepsilon|(\beta)$ is due to a decrease in $V_{zz}(\beta)$. On the other hand, ε is positive for subspectrum γ, and $|\varepsilon|(\gamma)$ is more than twice as large as $|\varepsilon|(\beta)$. These results indicate that the two sites in the HP phase can be assigned to five-coordinated Fe^{3+} ions which differ in the degree of structural distortion. The major fraction giving rise to the β subspectrum is less distorted than the minor fraction giving rise to the γ subspectrum. The hyperfine fields B_{hf} are barely pressure-dependent (Fig. 5c). A slight increase in B_{hf} in the pressure range of the phase transition is observed for component β. The values of $B_{hf}(\beta)$ in both the LP and the HP phase are similar to those of component γ, but considerably larger than for component α. In Fig. 6 the abundance of the three components calculated from the intensities with the assumption of equal f factors is given as a function of P. The fraction of the $Fe^{3+}(T)$ sites α decreases to zero between 6 and 13 GPa, simultaneously the fraction of the new component γ increases. In this pressure range also the fraction of component β increases with P. Therefore, in the HP phase the intensity ratio between the two subspectra is not 1:1 as in the LP phase, but about 3:1.

It is noted that on pressure decrease a substantial hysteresis is found. For decompression, spectra were measured at 11, 6, 4, and 1 GPa. At 11 and 6 GPa the spectra are still typical for the HP phase, at 4 GPa the coexistence of the three components is seen, and at 1 GPa the spectrum of the LP phase is recovered. This confirms the first-order nature of the pressure-induced B to TT structural phase transition in $Sr_2Fe_2O_5$.

3.3. *XRD Studies after Laser Annealing*

Experiments involving laser annealing of the HP phase were performed with the aim to investigate whether superstructure reflections show up in the XRD patterns that may be expected from the local structural changes indicated by Mössbauer spectroscopy. In Fig. 7 the XRD patterns at about 15 GPa before and after twofold laser annealing are compared. Note that argon was used as pressure medium which gives rise to the reflections marked by an asterisk in Fig. 7. The XRD pattern before laser irradiation is similar to

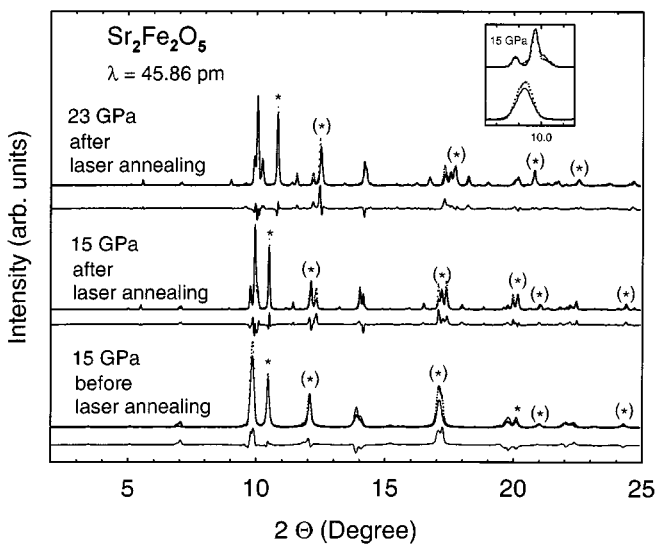

FIG. 7. Powder XRD patterns of $Sr_2Fe_2O_5$ from the laser-annealing experiments. Solid lines show results from Rietveld fits (R_{wp} between 0.20 and 0.25, esd's in lattice constants $\leq$ 0.2 pm). (Bottom) 15 GPa before laser annealing (a_{TT} = 379.5 pm, c_{TT} = 374.6 pm). (middle) 15 GPa after twofold laser annealing (a_{MN} = 538.7 pm, b_{MN} = 1049.8 pm, c_{MN} = 372.6 pm) (top) 23 GPa after laser annealing (a_{MN} = 530.4 pm, b_{MN} = 1028.8 pm, c_{MN} = 371.4 pm). The inset emphasizes the changes induced by laser annealing at 15 GPa in the 2Θ range of the strongest reflection. Reflections marked by an asterisk involve diffraction from the argon matrix (*, pure argon peak; (*), argon peaks overlapping with peaks from sample).

the 15 GPa diagram from the first set of experiments. The deviations between calculated and experimental intensities are, however, more pronounced than in the first set of experiments. From the quite spotted two-dimensional Debye–Scherrer patterns of the sample it is inferred that these deviations, which are also seen for the low-pressure B phase, are due to incomplete powder averaging within the sample volume exposed to the X-ray beam (30 μm in diameter).

Changes in the XRD diagrams after laser annealing evidence a further structural phase transition in $Sr_2Fe_2O_5$. This is particularly evident from the inset of Fig. 7 where the 2Θ region of the most intense reflections is emphasized. The XRD diagram of $Sr_2Fe_2O_5$ at 15 GPa after laser annealing is quite similar to an XRD pattern of $Sr_2Mn_2O_5$ calculated for $\lambda = 45.86$ pm with the structural parameters from Ref. (9). Accordingly, the structural model of $Sr_2Mn_2O_5$ (space group *Pbam*) was used as a starting point for describing the experimental patterns of $Sr_2Fe_2O_5$ after laser annealing. Final refinements included the scale factor, background parameters, lineshape parameters for $Sr_2Fe_2O_5$ and the pressure medium argon, a weight fraction for the argon contribution, the lattice parameters, and the positional parameters of the Sr and Fe atoms. In this way the main features of the experimental diagrams at 15, 20, and 23 GPa are reproduced (see Fig. 7). The remaining differences between experimental and refined patterns, in particular in the intensities, are possibly due to incomplete powder averaging. It is noted that, in contrast to the first set of experiments without laser annealing, the B structure is not totally recovered when pressure is released. The XRD pattern after pressure release implies the coexistence of B-type and $Sr_2Mn_2O_5$-type phase.

It is concluded that laser heating of $Sr_2Fe_2O_5$ at about 15 GPa leads to the transformation of the TT phase into a $Sr_2Mn_2O_5$-type (MN) phase where all transition metal ions are five-coordinated (see Fig. 1b). The main structural motif is a network of corner-sharing MO_5 square pyramids. The Sr^{2+} ions are coordinated by 10 O^{2-} ions. The orthorhombic cell parameters are related to the parameter a_P of a perovskite cell by $a_{MN} \approx \sqrt{2}a_P$, $b_{MN} \approx 2\sqrt{2}a_P$, $c_{MN} \approx a_P$ (9). The reduced volumes and lattice parameters $a'_{MN} = a_{MN}/\sqrt{2}$, $b'_{MN} = b_{MN}/2\sqrt{2}$, and $c'_{MN} = c_{MN}$ (included in Fig. 3) show that the transformation from the tetragonal into the $Sr_2Mn_2O_5$-type phase is accompanied by a further contraction of the structure. The additional decrease in volume is about $-1.5 \pm 0.5\%$ at 12 GPa. The pressure dependence of the lattice parameters of the MN phase reveals some anisotropy. The most prominent decrease with pressure occurs in b_{MN} whereas c_{MN} is only weakly pressure dependent.

3.4. Structural Considerations

For rationalizing the pressure-induced changes in the coordination environments of the Fe^{3+} ions it is instructive to compare the brownmillerite-type structure of $Sr_2Fe_2O_5$ with the structure of $Sr_2Mn_2O_5$ (see Fig. 1, note that the a_B, b_B, and c_B directions in the B structure correspond to the b_{MN}, c_{MN}, and a_{MN} directions in the MN structure). Both structures can be derived from the cubic perovskite by removing O^{2-} anions from alternate $[110]_c$ rows (8). For obtaining the B-type structure *all* O^{2-} ions in the $[110]_c$ rows are removed, but only in *every second* $(001)_c$ MO_2 plane of the cubic perovskite. This leads to a structure where one intact perovskite-like slab with MO_6 octahedra alternates with one slab with chains of MO_4 tetrahedra in the c direction of the orthorhombic lattice. In the $Sr_2Mn_2O_5$ structure *every second* O^{2-} ion in alternate $[110]_c$ rows is removed. Stoichiometry requires that this occurs in *every* $(001)_c$ MO_2 plane that leads to a square pyramidal environment of all the transition metal ions. These structural relationships suggest that the transformation of $Sr_2Fe_2O_5$ from the B-type into the MN phase under high pressure after laser annealing essentially involves breaking of one Fe–O–Fe bond in the perovskite-like $Fe^{3+}(O)$ layers and the motion of one O^{2-} ion into a vacant site of an adjacent $Fe^{3+}(T)$ layer (cf. Figs. 1a and 1b). Both, the $Fe^{3+}(O)$ and $Fe^{3+}(T)$ sites are transformed into five-coordinated sites. The formation of Fe–O–Fe bonds between Fe atoms in adjacent chains of tetrahedra in the B structure probably is the main reason for a better space filling in the $Sr_2Mn_2O_5$-type phase. As a consequence the values of b'_{MN} are much smaller than the a'_B values and a reduction in volume occurs (see Fig. 3). In addition the coordination number of the Sr^{2+} ions is increased from 8 in the B-type to 10 in the $Sr_2Mn_2O_5$-type structure. The structural changes are in agreement with the general rule in crystal chemistry that high pressure favors crystal structures with larger coordination numbers. However, the average coordination number of the Fe^{3+} ions is not increased.

Finally we are left with the question: which local structural changes occur due to the B to TT transformation under pressure at ambient temperature? The analysis of the Mössbauer spectra (Figs. 5 and 6) suggests that also the TT phase reveals only five-coordinated Fe^{3+} sites. Therefore it is expected that the B to TT transformation involves structural rearrangements similar to those that have been outlined above for the transformation into the $Sr_2Mn_2O_5$-type structure. In particular, breaking of one Fe–O–Fe bond in the perovskite layers leads to two five-coordinated Fe^{3+} sites that contribute to subspectrum β in the HP phase. However, the transfer of an O^{2-} ion into the adjacent $Fe^{3+}(T)$ layers seems to result in two structurally different Fe^{3+} sites, in contrast to the $Sr_2Mn_2O_5$ structure for which only one square-pyramidal Fe^{3+} site is expected. This is suggested by the observation of two subspectra in the HP phase that differ in the quadrupole interaction parameters ε. One of the sites possibly has a coordination environment equal to or similar to that of the two $Fe^{3+}(5)$ ions resulting

from the $Fe^{3+}(O)$ sites. It only increases the fraction of subspectrum β, but does not give rise to a separate signal in the Mössbauer spectra. The other site appears to be more distorted which may arise from a longer distance between the central ion and the transferred O^{2-} ion. Taking into account the area fractions in the Mössbauer spectra the changes in the coordination environments of the Fe^{3+} ions in the course of the B to TT transformation may be summarized as

$$2Fe^{3+}(T) + 2Fe^{3+}(O) \rightarrow 3Fe^{3+}(5, \beta) + 1Fe^{3+}(5, \gamma). \quad [3]$$

The decrease in volume again mainly is the consequence of a contraction due to the formation of Fe–O–Fe bonds between chains of adjacent tetrahedra. The smaller lattice parameter c_{TT} then corresponds to b'_{MN} in the MN phase.

The TT phase formed above 11 GPa at room temperature probably is metastable. Its local structure reveals essential features of the $Sr_2Mn_2O_5$ structure. Incomplete relaxation of the atoms and disorder of oxygen ions lead to an average perovskite-like XRD pattern. Heating of the TT phase by laser annealing enhances the mobilities of the atoms and allows them to move into the positions typical for the $Sr_2Mn_2O_5$-type structure which is thermodynamically stable in this pressure range.

4. CONCLUSIONS

We have established two structural phase transitions in $Sr_2Fe_2O_5$ under high pressure by combining angle-dispersive powder X-ray diffraction and ^{57}Fe Mössbauer experiments. The ambient-pressure brownmillerite-like phase, which has a defect perovskite structure with an ordered arrangement of oxygen vacancies, is transformed into a tetragonal perovskite-type phase above ≈ 10 GPa. The transition is of first order. Laser annealing of this phase induces the formation of a phase that is isostructural to the Mn^{3+} analog $Sr_2Mn_2O_5$. The most important result from our study is the complete transformation of the tetrahedrally and octahedrally coordinated Fe^{3+} sites of the ambient pressure structure into five-coordinated $Fe^{3+}(5)$ sites under high pressure. On a local level the main difference between the tetragonal and the $Sr_2Mn_2O_5$-type phase appears to be the presence of two structurally different $Fe^{3+}(5)$ sites in the former in contrast to only one $Fe^{3+}(5)$ site in the latter. The mechanism of the phase transitions can be rationalized by considering breaking and forming of Fe–O–Fe bonds in the octahedral and adjacent tetrahedral Fe–O layers of the brownmillerite-type structure, respectively.

ACKNOWLEDGMENTS

We thank U. Oelke for experimental support with the synchrotron experiments, W. Hölle for assistance with sample preparation and characterization, and I. Loa for helpful discussions. This work was supported by the German-Israel Science Foundation, Grant I086.401.

REFERENCES

1. E. F. Bertaut, P. Blum, and A. Sagnières, *Acta Crystallogr.* **12,** 149 (1959).
2. P. K. Gallagher, J. B. MacChesney, and D. N. E. Buchanan, *J. Chem. Phys.* **41,** 2429 (1964).
3. C. Greaves, A. J. Jacobson, B. C. Tofield, and B. E. F. Fender, *Acta Crystallogr. B* **31,** 641 (1975).
4. M. Harder and Hk. Müller-Buschbaum, *Z. Anorg. Allg. Chem.* **464,** 169 (1980).
5. P. K. Gallagher, J. B. MacChesney, and D. N. E. Buchanan, *J. Chem. Phys.* **43,** 516 (1965).
6. M. Parras, L. Fournes, J.-C. Grenier, M. Pouchard, M. Vallet, J. M. Calbet, and P. Hagenmuller, *J. Solid State Chem.* **88,** 261 (1990).
7. X. D. Zou, S. Hovmöller, M. Parras, J. M. González-Calbet, M. Vallet-Regí, and J. C. Grenier, *Acta Crystallogr. A* **49,** 27 (1993).
8. K. R. Poeppelmeier, M. E. Leonowicz, J. C. Scanlon, J. M. Longo, and W. B. Yelon, *J. Solid State Chem.* **45,** 71 (1982).
9. V. Caignaert, N. Nguyen, M. Hervieu, and B. Raveau *Mater. Res. Bull.* **20,** 479 (1985).
10. J. A. Alonso, M. J. Martínez-Lope, J. L. García-Muñoz, and M. T. Fernández, *Phys. B* **234–236,** 18 (1997).
11. S. Shin, M. Yonemura, and H. Ikawa, *Mater. Res. Bull.* **13,** 1017 (1978).
12. J.-C. Grenier, N. Ea, M. Pouchard, and P. Hagenmuller, *J. Solid State Chem.* **58,** 243 (1985).
13. Y. Takeda, K. Kanno, T. Takada, O. Yamamoto, M. Takano, N. Nakayama, and Y. Bando, *J. Solid State Chem.* **63,** 237 (1986).
14. L. Fournes, Y. Potin, J. C. Grenier, and P. Hagenmuller, *Rev. Phys. Appl.* **24,** 463 (1989).
15. M. Takano, T. Okita, N. Nakayama, Y. Bando, Y. Takeda, O. Yamamoto, and J. B. Goodenough, *J. Solid State Chem.* **73,** 140 (1988).
16. P. Berastegui, S.-G. Eriksson, and S. Hull, *Mater. Res. Bull.* **34,** 303 (1999).
17. A. Hammersley, Computer Program Fit2D, ESRF, Grenoble, 1997.
18. J. Rodriguez-Carvajal, "FullProf: A Program for Rietveld Refinement and Pattern Matching Analysis," Abstracts of the Satellite Meeting on Powder Diffraction of the XV Congress of the IUCr, p. 127, Toulouse, 1990.
19. A. C. Larson and R. B. von Dreele, General Structure Analysis System (GSAS), Los Alamos National Laboratory, Report No. LAUR 86-748 (1990).
20. R. A. Young, *in* "The Rietveld Method" (R. A. Young Ed.), Oxford Univ. Press, Oxford, 1993.
21. R. W. Grant, *J. Chem. Phys.* **51,** 1156 (1969).